Peer-reviewed version available at *Materials* **2019**, *12*, 172; doi:10.3390/ma12010172

Study of the Microstructure and Crack Evolution Behavior of Al-5Fe-1.5Er alloy

Ming Li* , Zhiming Shi, Xiufeng Wu, Huhe Wang, Yubao Liu
College of Materials Science and Engineering, Inner Mongolia University of Technology, Hohhot 010051, PR China

Abstract: The microstructure of Al-5Fe-1.5Er alloy was characterized and analyzed by using XRD, SEM, TEM and EDS. The effect of microstructure on the behavior of crack initiation and propagation was investigated by in situ tensile testing. Results show that the microstructure consists of α-Al matrix, Al_3Fe, Al_4Er, eutectic phase Al_3Fe + Al_4Er, while the 1.5 wt.% Er was added in Al-5Fe alloy. The twin structure of the Al_3Fe phase was observed, and the twin plane is {001}. Moreover, a continuous concave and convex interface structure of the Al_4Er has been found. Al_3Fe is in the form of a sheet with a clear gap inside.In situ tensile tests of the alloy at room temperature show that the crack initiation occured mainly in the Al_3Fe phase, and that the crack propagation modes include intergranular and transgranular expansion. Crack transgranular expansion is due to the strong binding ability between Al_4Er phases and surrounding organization, and the continuous concave and convex interface structure of the Al_4Er provides a significant meshing effect on the matrix and eutectic structure.

Key words: Al-5Fe-Er alloy; microstructure; in situ tension; crack evolution

As the lightest structural material, Aluminum alloy has the advantage of low density, high specific strength and stiffness, good thermal conductivity as well as excellent electromagnetic shielding and anti-radiation properties, thus widely used in manufacturing, aerospace, electronic communication and other fields[1-4]. Although 8000 series aluminum alloy is the most widely used casting aluminum alloy in industrial production, the poor mechanical properties at room temperature is one of its bottleneck for further application and development. Alloying effect is one of the effective means to improve the mechanical properties of aluminum alloy. The existing research[5-13] has shown that rare earth Er can improve the mechanical properties of aluminum alloy . After adding rare earth Er, a stable structure of rare earth aluminum compounds can form in the alloy, which can inhibit the precipitation of Al_3Fe phase. At present, researchers have carried

* Corresponding author. Tel.: +86 15184726161, Fax.: +86 0471 6575752
E-mail address: nmgclxylm@imut.edu.cn(M. Li)

out a lot of experimental work on the improvement of microstructure and mechanical properties of 8000 series aluminum alloy after adding rare earth Er. The research findings are as follows: Karnesky [8-14] et al found that the microstructure of 8000 series aluminum alloy was refined due to the addition of Er (0-0.8wt.%) and formed new granular or needle like Al4Er compounds. The study of Che, Hongmei[15-19] suggests that the Al_4Er phase precipitated at grain boundaries increases the mechanical properties of 8000 series aluminum alloy after the addition of Er to 0.3-1.0wt.%. Tong Dorin [20-26] et al reported that the Al_4Er phase was formed in 7073 after the addition of 1wt.% Er, and both the tensile strength and yield strength of the alloy were improved after alloying.

At present, there are few research on the crack propagation behavior of 8000 series aluminum alloy conducted from the perspective of in situ observation. Based on the previous experiments, this paper adopted the in situ dynamic observation of scanning electron microscope technique to study the crack initiation and Crack propagation behavior of Al-5Fe-1.5Er alloy at room temperature. The paper also discussed the influence and mechanism the microstructure has on the crack evolution.

1 Test Methods and Procedures

The pure aluminum、Al-15%Fe and Al-10%Er intermediate alloy were used as raw material to prepare Al-5Fe-1.5Er alloy by vacuum induction melting furnace. During the smelting process, the alloy was kept in the vacuum, protected by argon, and then shaped by metal mould casting. The HCS-140 high frequency infrared ray carbon sulphur analyzer was employed to analyze the composition of the alloy. By using S-3400N scanning electron microscope (SEM) and its corresponding energy spectrometer, the microstructure and fracture appearance of the test alloy was observed, the composition and content of the elements in each phase was analyzed. X-ray diffraction (XRD) phase analysis was conducted by using the D/MAX-2500/PC type X-ray diffractometer produced by Rigaku Corporation. The TEM samples of the alloy were prepared by Gatan691 precision polishing system. The JEM2010 transmission electron microscope (TEM) and its corollary energy dispersive spectrometer is applied in analyzing the microstructure and energy dispersive spectrum analysis (EDS) of the testing alloy.

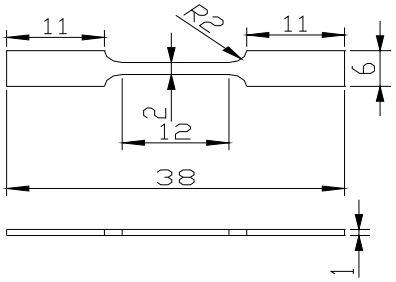

Fig. 1 Geometry and size of tensile specimen

The specimen size of in situ tensile at room temperature is shown in figure 1. After the mechanical grinding and electrolytic polishing on the prefabricated gap of the alloy, the alloy is put to in situ tensile test on the tensile stage under FEI Quanta 650 scanning electron microscope （SEM）vacuum environment. The operating rate is set to 0.5mm/min.

2 Results and Discussion

2.1 XRD and SEM Results Analysis

The XRD result of test alloy is shown in figure 2a. Through PDF card analysis, the main phase compositions are detected, including α-Al, Al_3Fe,Al_4Er and $Al_{10}Fe_2Er$. Figure 2b is a picture of the test alloy SEM. The EDS results analysis on the selected points is shown in table 1. It can be seen that the morphology of the iron phase in the alloying tissue changed significantly due to the addition of rare earth elements ,when the amount of rare earth added was 1.5 Wt. Point E is Al matrix, and a small little amount of Fe element is dissolved in the matrix. The main alloying elements of point B island phase contain Al, Er, Fe. Removing the influence of Fe element content, point B is regarded as η-Al_4Er phase. The particle phase at point A are mainly composed of Al ,Fe elements, regarded as θ-Al_3Fe phase. The white needle-like phase at point C are mainly composed of Al ,Fe and Er elements. Referring to results of XRD, the phases maybe confirmed as $Al_{10}Fe_2Er$. Further observation on the results of SEM alloy found that there were eutectic structure formed by the Al_4Er and its peripheral α-Al in the alloy. Moreover, part of white needle-like phase $Al_{10}Fe_2Er$ at grain boundaries attaches itself to η-Al_4Er phase. Part of needle-like phases precipitate inwardly to the matrix.

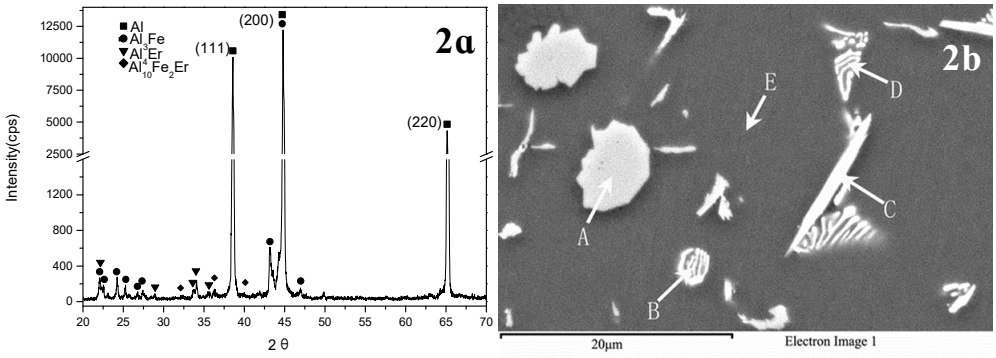

Fig.2 XRD analysis (a) and SEM image (b) of the as-cast alloy

Tab. 1The EDS analysis of the phases in test alloy

element（wt%）	Al	Fe	Er
A	62.66	37.34	—
B	82.38	0.64	16.98
C	65.94	15.14	18.91
D	81.96	—	18.05
E	100	—	—

2.2 TEM Result Analysis

The Al_3Fe phase is bottom center monoclinic structure, Its lattice constant is a=1.549nm、b=0.808nm、c=1.247nm and β=107.72°。The TEM picture of the Al_3Fe phase in the test alloy and the result of the selected area electron diffraction pattern (SAED) are shown in figure 3. Figure 3a is the picture of the morphology of the second-phase obtaining by electrolyzation. Further observation of the second-phase θ-Al_3Fe and η-Al_4Er phase in figure 3b, It can be seen that It can be seen that θ-Al_3Fe, η-Al_4Er combine to grow together.. The result of the selected area electron diffraction pattern (SAED) about θ-Al_3Fe and η-Al_4Er phase in figure 3b is shown in figure 3c and figure 3d respectively. After calibration for the two sets of selected area electron diffraction patterns, the η phase is proved to be Al_4Er, with the zone axis orientation being [130](Fig. 3c) ;and the θ phase is proved to be Al_3Fe, with the zone axis orientation being$[\bar{1}02]$ (Fig. 3d) respectively. This result further verifies the SEM and EDS results of the white needle-like phase phase is eutectic phase η+θ..

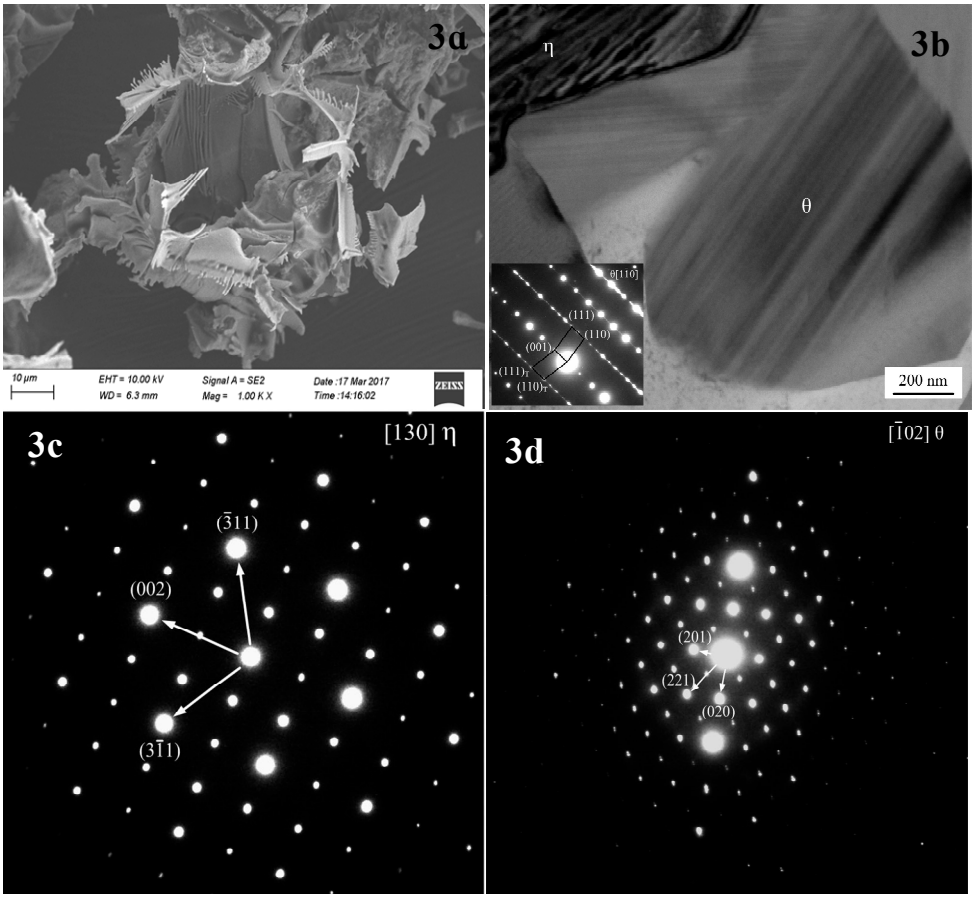

Fig. 3 TEM image of the second-phase (a) and partial enlargement map (b) and SAED pattern of the Al_4Er in [130] zone axis (c) and the Al_3Fe in[$\bar{1}02$] zone axis (d)

Figure 3b indicates that a mass of plane defects penetrates the whole θ-phase grain along the growth direction. According to the SAD pattern in Fig.3b the plane defects are considered to be twin crystal and stacking fault[27-30]. The twin crystal appears in the (001) plane, and a mass of stacking fault in θ-phase leads to the appearance of streaks in the SAD pattern. The HREM morphology of the twin crystal is shown in Fig. 4a. High-density regular twinning is evident in the θ-crystal. The HREM image shows a complex atomic arrangement, and the twinning is difficult to distinguish, as presented in Fig. 4b. However, the adjacent atomic arrangements are slightly different along the (001) plane after serious analysis and comparison, thereby confirming the atomic arrangements of twinning in Fig.4b. The formation of (100) and (201) twinning may require more energy than (001) twinning. The nucleus contains only (001) twinning and stacking faults, and the other twinning routes are suppressed. The (110) and $(110)_T$ planes formed by (001) twinning offers a mass of steps favoring atomic stacking along the (001) plane and leads to the continuous growth of (001). Notably, twinning nucleation may appear and grow in the growing θ-crystal, and (001) twinning remains to be the sole mechanism.

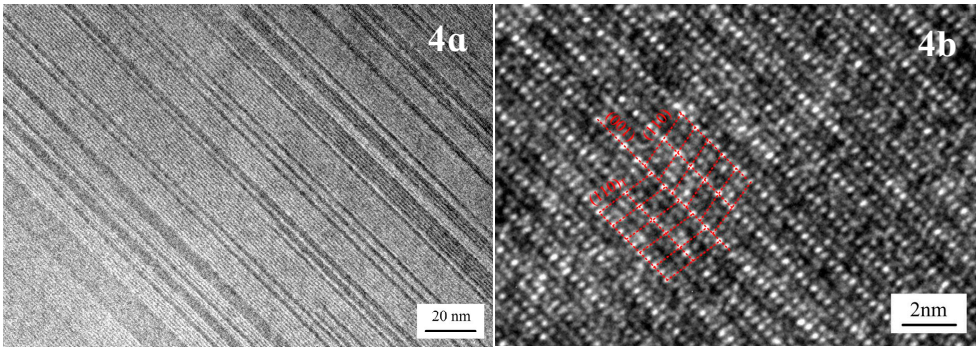

Fig.4 Highdensity twin morphology (a) and HREM image of (001) twinning of the Al_3Fe phase

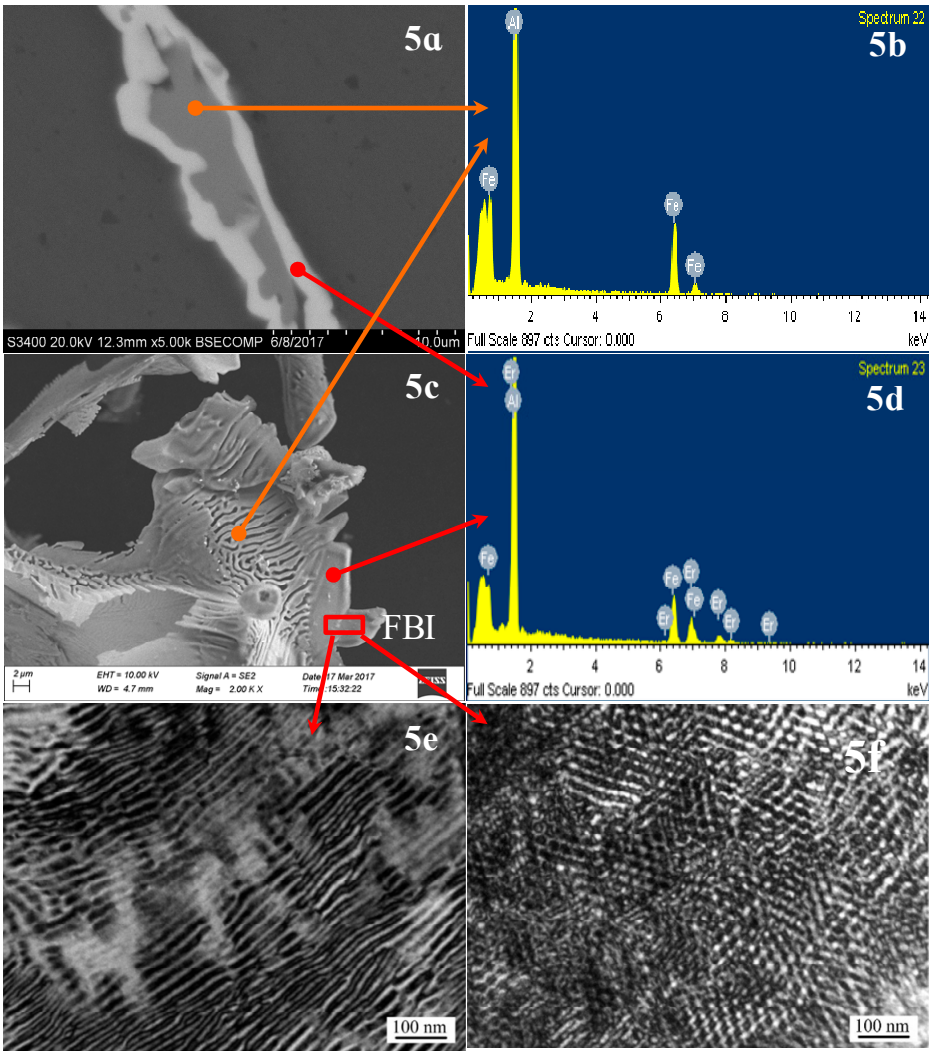

Fig. 5 The TEM images, SEM and EDS of Al_4Er phase a、c. SEM image of Al_4Er in grain boundary b、d. EDS analysis e、f.TEM image of Al_4Er in grain

The existence of twin structure in Al_3Fe may result from the high structural stress in the alloy. Metal casting has a relatively fast cooling rate. When the alloy is cooled to room temperature, the structural stress in the alloy is in an unbalanced state and has a tendency to release spontaneously. When the stress exceeds the critical shear stress of Al_3Fe phase, the twin structure Al_3Fe phase is

induced to form.

η-Al_4Er phase is an cubic structure, and its lattice constant is (a=0.4215nm, , α=β=γ=90°). Figure 5 shows the TEM、EDS and SEM result of Al_4 Er phase. Figure 5a is a picture of needle phase SEM at grain boundary. According to the result of needle-like phase EDS in figure 5b and figure 5d, the proportion of Al and Er element contents in the outer edge of phase is relatively large. The calibration of the selected area electron diffraction pattern (SAED) on the needle-like phase prove it to be Al_4Er phase, with [130] being the zone axis orientation (Fig.3c) , which is consistent with the result of needle-like SEM and EDS. Further investigation revealed that the grain boundaries of the needle-like Al_4Er phase is coated on the outside side of Al_3Fe. We came to the conclusion that $Al_{10}Fe_2Er$ is a composite phase, the outer layer is Al_4Er, and the inner layer is Al_3Fe , which can be identified as θ-Al_3Fe/ η-Al_4Er.The end face of the needle-like Al_4Er is parallel with the bonding interface of α-Al matrix along the length direction, and is intermittent along the width direction exhibiting an obvious concave convex appearance. At this moment, Al_4Er starts the adsorption growth along the width direction, namely, along the width direction, all the atoms on the concave convex interface will combined into the crystal, thus the crystal, even in a small undercooling, can grow up quickly. However, the uneven degree of diffusion of Al and Er atoms on the concave convex interface of Al_4Er front edge result in the formation of wall-like Al_4Er. The change in the interfacial morphology of Al_4Er reflects the needle-like Al_4Er phase tends to grow into short rod-like shapes. Figure 5c is the SEM image of the needle-like phase Al_4Er and Al_3Fe inside the grain. It can be seen that two phases grow perpendicular to each other, so the dense Al_4Er phase hinders the diffusion of iron and inhibits the growth of Al_3Fe. The shape of smooth edge needle-like Al_4Er phase is in good agreement with Al matrix. The η- Al_4Er exhibits evident fibrous characteristics, as observed from two zone axes under TEM presented in Figs. 5e and 5f. The average distance of fibers is approximately 20nm. The η-phase should be disordered during the generation process of alloy phase because of attached growth . The η- Al_4Er is the dominant reaction product and performs an important role to control the the generation process of alloy phase in molten aluminum. In addition, the finger-like morphology of the η- Al_4Er was attributed to the distinctive crystal structure; the orthorhombic structure consists of 30% vacancies along the c-axis [001], which offers a rapid diffusion path. However, a η-phase attached growth means that all atomic positions in the lattice are same. No 30% of vacancies along the c-axis [001]

are offered, there were many dislocation line inside of the Al_4Er phase and the phase is proved to be brittle phase.

2.3 The Results Analysis of In Situ Tensile Test at Room Temperature

The process of the alloy in situ tensile at room temperature is shown in figure 6. Figure 6a shows the relation curve between the load and displacement curves of the alloy specimens. The in situ tension process observation starts from the position of the arrow in the diagram. The tensile scan images of the different corresponding positions are shown in figure 6 (b-o). Figure 6b is the back-scattered electron scanning images of the specimen when the external load reaches 200N. At the moment, the specimen is in the elastic deformation stage, and for the position of the sample reserved gap front, no crack source has formatted. When the load keeps to increase (Figure 6c), micro crack source began to form in the gaps of the specimen due to stress concentration. No significant change is found in the middle part of the specimen. A close magnification of the selected area in figure 6c(Figure 6d) clearly shows that a large number of second phases, i.e. needle-like θ-Al_3Fe+η-Al_4Er, particle Al_3Fe phase, island-like Al_4Er dispersively distributed in the α-Al matrix of alloy specimen. Moreover, the microstructure of the alloy is dense. Select the elliptic region A and B (divorced eutectic Al_3Fe+ Al_4Er phase) in figure d as a comparative observation area. Continue to increase the external load (Fig. 6e), the cracks of the gap grows. Due to the effect of stress concentration, some Al_3Fe phase at the front of the crack source (the magnified area in figure 6e) and in the middle of the specimen begin to generate fine cracks. For the time being, no obvious plastic deformation characteristics was observed in the central picture of the specimen (figure 6f, a selected area from figure 6e), and no microcrack formation is found in aluminum compounds. Continue to increase the external force, the main crack expanded rapidly (figure 6g). There were an obvious slip bands and secondary cracks on both sides of the main crack. The formation of secondary cracks is a result of the further expansion of the micro cracks in Al_3Fe/Al4Er phase. Enlarge the selected areas in figure 6g(figure 6h), one can see the widen micro cracks formed by the broken island-like phase Al_4Er on both sides of the main crack. The needle-like phase Al_3Fe/Al_4Er and granular Al_3Fe phase are broken. Al_3Fe/Al_4Er cracked several times along the length direction. The width of micro cracks formed by the broken rare earth aluminide rupture is relatively small, and the bonding between the rare earth aluminum compounds and the interface of the matrix is good, which indicates that the needle-like

Al_3Fe/Al_4Er phase and particle Al_4Er phase in the alloy can effectively resist the external load changes. In addition, the movement of the slip line is hindered by the rare earth aluminide, which further improves the tensile strength of the alloy. With the tension continues, the front part of the main crack front showed a "Z" - shaped expansion (see from the selected area in the figure 6i in the selected block area) and next to the front of the main crack, an obvious plastic deformation region (slip band formation) appeared in the matrix. When the main crack expanded to the area, the crack path extended forward along the slip plane (steps), thus forming the front end of "Z" shape crack. This kind of winding crack propagation can improve the fatigue strength of alloy [12]. The Z shaped crack continues to expand forward. When the crack passed grain 1 and grain 2, one can see from the path of the main crack that there are two forms of crack expansion, i.e. transgranular and intergranular. The micro cracks that near the main crack grain are connected to each other, expanding a pathway for its extension. When the main crack expand to the grains 3, it didn't extends forward along the grain boundary but the transgranular went through the grain interior instability region (see the area surrounded by the blue curve in figure 6j). The red arrow in the diagram points to the direction of crack propagation. the particle Al_3Fe phase in the coarse $\theta+\eta$ eutectic structure at the grain boundary (the area selected by yellow lines) is broken. And the weak bonding ability between the eutectic structure and the matrix interface led to cracks and separation of the two. Further observation revealed that formation of the needle-like phase Al_3Fe/Al_4Er and particle Al_4Er phase formed at the grain boundary made eutectic structure and matrix connected closely together, especially the concave and convex interface structure of Al_4Er increases its meshing area with the surrounding tissue, which further hindered the separation between the primary crystal α-Al and Al element in the eutectic structure. The step is to block the Al from the αAl and the eutectic structure. Therefore, the interface needs to provide a larger external load to initiate and propagate cracks, which results in transgranular cracking of the main crack. Continue to increase the external force, the stress concentration area exists in front of the main crack, making the surface of the sample unstable (the selected region C and D in figure 6k). There are slip bands of different orientation in the region.Further observation on the fracture behavior of crack through the selected region C and D (figure 6m and figure n) found that in figure 6m, each piece of Al_3Fe/Al_4Er and matrix interface bond closely and slides along the direction of deformation for some distance, which shows that the bonding strength between the needle-like

Al_3Fe/Al_4Er and the matrix interface has hindered the slip of the matrix, forcing the need-like phase break into several segments of almost the same length（about 2μm）along the length direction.

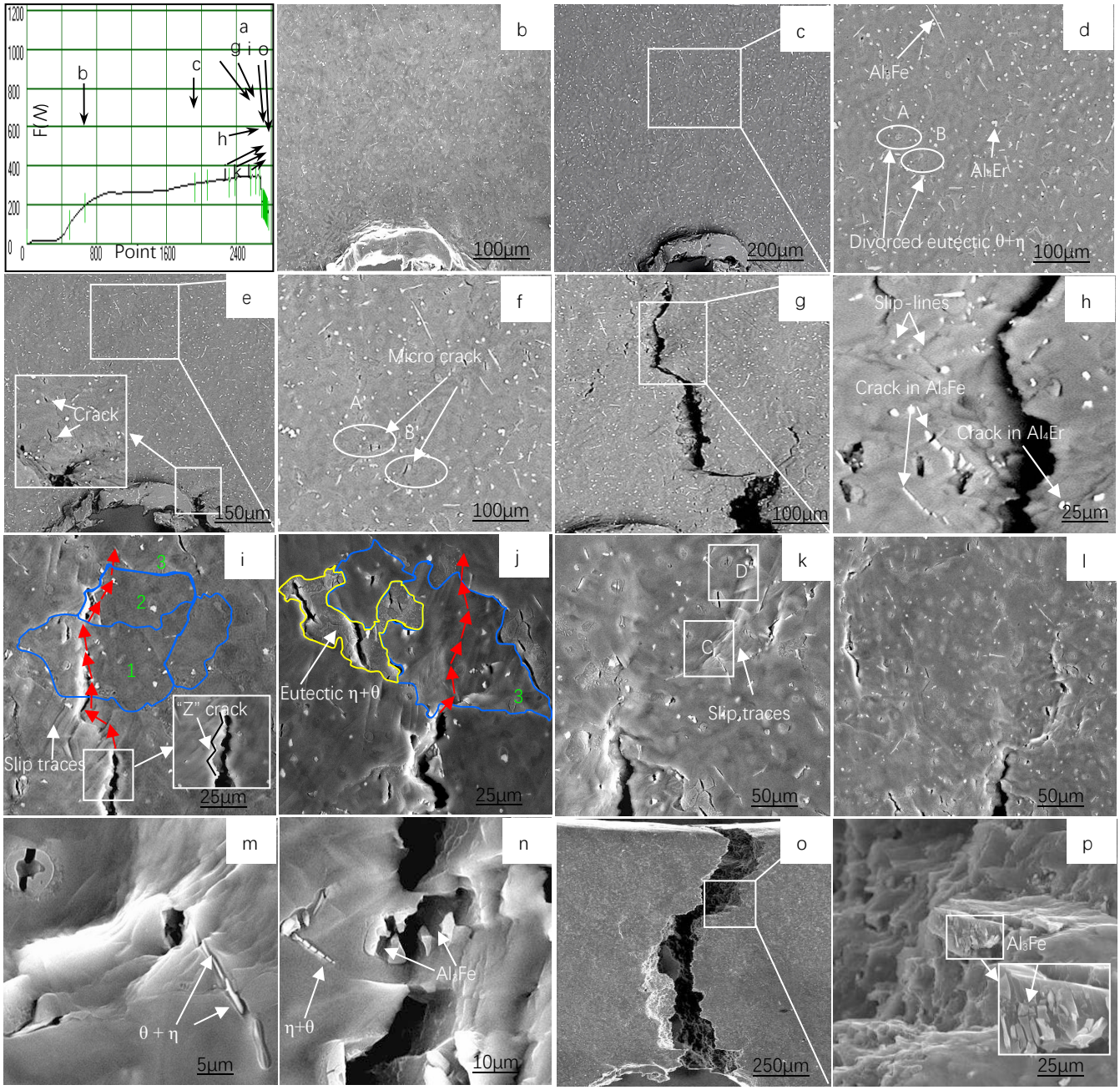

Fig. 6 The in situ tension test of the alloy at room temperature

(a) Load-position curve; (b) SEM image of the position b in fig.a ;(c) SEM of the position c in fig.a ; (d) the enlarge image of selected area in fig. c; (e) SEM image at F=340N; (f) the enlarge image of selected area in fig. e; (g) (h) (i) (j) (k) (l) SEM images of the position g, h, i, j, k, l in fig.a; (m) the enlarge image of selected area C in fig. k; (n) the enlarge image of selected area D in fig. k; (o)SEM image of fractured specimen; (p) the enlarge image of selected area in fig. o

Preprints (www.preprints.org) | NOT PEER-REVIEWED | Posted: 20 November 2018 doi:10.20944/preprints201811.0481.v1

Peer-reviewed version available at Materials 2019, 12, 172; doi:10.3390/ma12010172

The fracture is mainly caused by the stress concentration that the convex and concave interface of Al_4Er bore, the force of which is stronger than the bond strength between the Al_3Fe/Al_4Er eutectic structure and the matrix. The crack in figure 6n to continue to move forward and go through the unstable region, making the brittle hardness phase Al_3Fe break and separate. Increase the tensile strength and the alloy specimen fractures quickly. The surface of specimen fracture (figure 6o) along the crack direction is non-homogeneous. Further observation of the selected region in the fracture (figure 6p) found the black hole at the bottom right should be caused by the fractured phase Al_3Fe. The nearby residual of Al_3Fe is exposed in the above the surface of the fracture matrix on the right side of the main crack, and fractures along the direction of the stress, which shows that the main crack produced a secondary micro cracks going through the large size Al_3Fe. Under the external force, the secondary micro cracks extend to the nearby Al_3Fe phase, releasing the stress concentration produced by Al_3Fe and the surrounding matrix. The micro cracks continue to propagate to the matrix. Under the effect of sheer stress, the matrix form into slippage step and converges to form dimples at the edge of the matrix slippage step through the extension of micro cracks of Al_3Fe_2, whereas, the effect of cross-slip will lead to the formation of a tear ridge at the fracture surface.

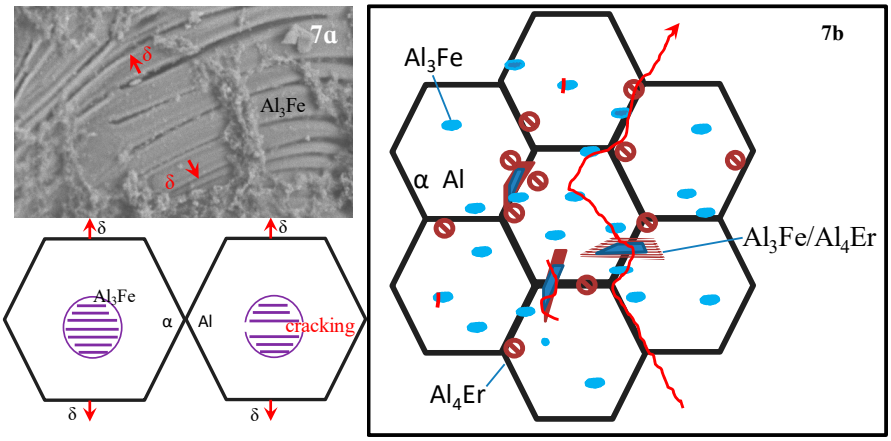

Fig.7 Schematic diagram of crack propagation in the Al3Fe(a) and in the alloy(b)

Figure 7 is a schematic diagram of the crack propagation path. Since the Al_3Fe at the grain boundary can easily initiate micro cracks, the Al_3Fe/Al_4Er eutectic structure breaks when the main crack passes. The bonding ability between Al_3Fe and matrix interface is weak, thus causing detachment of the two, making the cracks extend along the grain boundaries. When the rare earth aluminide is precipitated from the eutectic structure at grain boundaries, the compounds have a better effect on the meshing between the eutectic structure and the matrix, improving the

mechanical stability of the eutectic structure at grain boundaries, resulting in the formation of unstable region inside the grains, and casing the expansion of the transgranular crack.

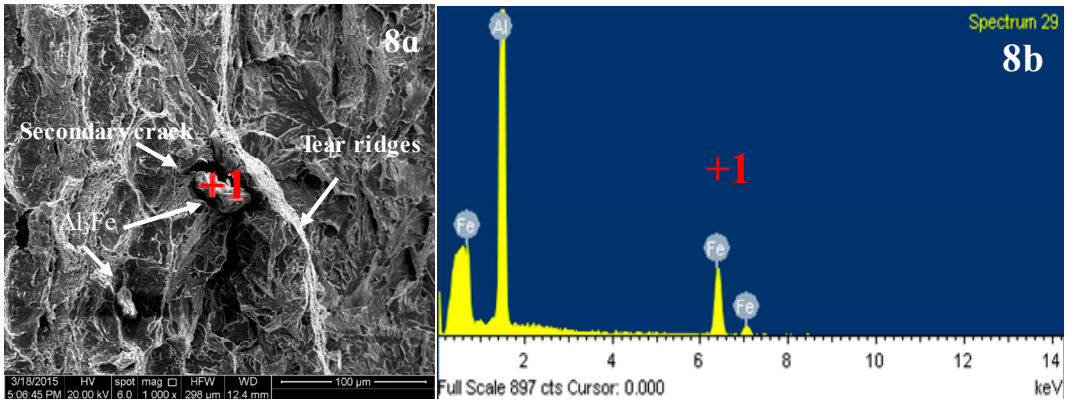

Fig. 8 SEM image (a) and EDS analysis (b) of the alloy

The analysis on EDS test results of the selected point from the fracture surface (figure 8b) found that the point includes Al, Fe and Er, indicating it is on the grain boundary. Therefore, the fracture mode of the alloy is a combination of intergranular fracture and quasi cleavage fracture.

3 Conclusions

(1) The main phase composition of Al-5Fe-1.5Er alloy includes α-Al matrix, Al_4Er, eutectic phase $Al_{10}Fe_2Er$; Al_3Fe phase.is needle-like and particle. There is a twin structure in Al_3Fe, with the twin plane being {001}. Al_4Er has a concave and convex interface structure. $Al_{10}Fe_2Er$ is a composite phase, the outer layer is Al_4Er, and the inner layer is Al_3Fe , named as θ-Al_3Fe/ η-Al_4Er

(2) In situ tensile test at room temperature shows that the crack are mainly formed inside the coarse particle Al_3Fe and mode of crack propagation include the crack growth mode includes intergranular expansion and intergranular propagation. Intergranular propagation is the result of the strong binding ability between the phase distributed along the grain boundaries, Al_4Er, and the surrounding interface. The pinning effect is remarkable. The concave and convex interface structure of the Al_4Er has a strong meshing effect on the eutectic structure and the matrix, which improves the mechanical stability between the eutectic structure at grain boundaries and the interface of the matrix.

Acknowledgments

The authors gratefully acknowledge financial support from the National Natural Science Foundation of China (No. 51661026).

References

[1]Wang, X., Guan, RG. & Wang, Y. Metall and Materi Trans B. 49 (2018) 2225–2231.

[2] Moustafa, M.A..J. Mater. Proc. Technol. 209(2009) 605–610.

[3]Çadirli, E., Tecer, H., Sahin, M., Yilmaz, E., Kirindi, T Gündüz, M.J.Alloys Compd., 632(2015) 229–237.

[4]Booth-Morrison, C., Seidman, D. N., Dunand, D.C..Acta Mater.. 60(2012)3643–3654.

[5]Belov, N.A., Korotkova, N.O., Alabin, A.N. Russ. J. Non-ferrous Metals. 59 (2018)276–283

[6] Q.R. Zhao, Z. Qian, X.L. Cui, Y.Y. Wu, and X.F. Liu:J. Alloys Compd., 650(2015) 768–776.

[7] R.G.Guan,Y.F.Shen,Z.Y.Zhao,X.. J. Mater. Sci. Technol.33(2016) 215-223.

[8]Karnesky, Richard A.; Dunand, David C.; Seidman, David N. ACTA MATER.. 57(2009) 4022-4031

[9] S. Miyazakia, A. Kawachib, S. Kumaia, A. Satoa.Mater. Sci. Eng. A, 400–401 (2005) 294-299.

[10]J.M.Cubero-Sesin,Z..Metall. Mater. Trans. A,43(2012)5182-5192.

[11]S.S. Nayak, B.S. Murty, S.K. Pabi. Bull. Mater. Sci., 31 (2008) 449-454.

[12] Seidman, David N.Karnesky, Richard A.; Dunand, David C. Acat Mater. 57(2009) 4022-4031.

[13] R.A. Mesquita, D.R. Leiva, A.R. Yavari, W.J. Botta Filho.Mater. Sci. Eng., A, 453 (2007), pp. 161-169.

[14] E.A. Starke, J.T. Staley.Prog. Aero. Sci., 32 (1996)131-172.

[15] Che, Hongmei; Jiang, Xianquan; Qiao, Nan; et. al.. J. Alloys Compd.., 708(2017),P P: 662-670.

[16] Feng, J; Huang, WD; Lin, X. J Crys G. 197(1999)393-398.

[17] Goulart, Pedro R.; Cruz, Kleber S.; Spinelli, Jose E. J. Alloys Compd..470(2009) 589-599.

[18] TRIVEDI, R; KURZ, W . Int Mater Rev.39(1994) 49-74.

[19] P.R. Goulart, K.S. Cruz, J.E. Spinelli, I.L. Ferreira, N. Cheung, J. Alloy. Compd., 470 (2009) 589-599

[20] T. Dorin, N. Stanford, N. Birbilis, R.K. Gupta. Sci., 100 (2015) 396-403.

[21] Wen, S. P.; Gao, K. Y.; Huang, H.; J. Alloys Compd.574(2013)92-97.

[22] Zhang, Y; Gao, K. Y; Wen, S. P; J. Alloys Compd. 610(2014) 27-34.

[23] Fuller, CB; Seidman, DN; Dunand, DC . Acta Mater.. 51(2003) 4803-4814

[24] Y. Harada, D.C. Dunand.Intermetallics, 17 (2009) 17-24.

[25]A.M.Samuel,G.H.Garza-Elizondo,H.W.Doty,F.H.Samuel.Mater. Des..80(2015)99-108

[26] U. Prakash, G. Sauthoff. Intermetallics, 9 (2001) 107-112.

[27] H. Sasaki, K. Kita, J. Nagahora, A. Inoue.Mater. Trans., 42 (2001)1561-1565

[28] FREIBURG, C; GRUSHKO, B. J. Alloys Compd.210(1994) 149-152

[29] Zhang, LM; Schneider, J; Luck, R.INTERMETALLICS. 13(2005)1195-1206.

[30] Wu, M.X.; Liu, T. Dong, M. J. Alloys Compd. 121(2017)138-144.